



Application of position and inertial-rate control to a 2-DOF gyroscopic platform

Francisco R. Rubio^{*}, Manuel G. Ortega, Francisco Gordillo, Manuel Vargas

Depto. Ingeniería de Sistemas y Automática, Escuela Superior de Ingenieros, Universidad de Sevilla, Camino de los Descubrimientos s/n, 41092 Sevilla, Spain

ARTICLE INFO

Article history:

Received 12 October 2008

Accepted 23 November 2009

Keywords:

Inertial platform

Adaptive control

Gain scheduling

Friction compensation

ABSTRACT

This paper presents a control application for the inertial stabilization of a gyroscopic platform with two degrees of freedom (2-DOF). The purposes of this application are, first, to control the angular positions of the platform in the absence of inertial disturbances and second, to control velocities measured in an inertial frame, while rejecting the disturbances associated with moving components. With regard to the first objective, a switching-control strategy is proposed in order to reduce the effects of friction as the main source of undesirable non-linear behaviors. Regarding the inertial-rate control, a master–slave control structure is suggested to achieve the desired specifications. Simulation and experimental results are presented, showing the performance attained on a real platform.

© 2009 Elsevier Ltd. All rights reserved.

1. Introduction

In this paper, we discuss the design and implementation of a control strategy for a gyroscopic platform whose position and inertial velocity in the presence of perturbations need to be regulated. There are some applications that require accurate positioning and low velocity tracking. In these cases, friction phenomena usually have significant effects, leading to follow-up errors and the appearance of limit cycles. These errors need to be compensated for or reduced to fulfill the specifications in each case.

Some related applications can be found in the literature. In Guesalada [7], a controller for a positioning servo that takes into account friction phenomena is presented. A gain-scheduled control of systems with dynamic friction is proposed in Vivas et al. [16]. Switching controllers for tracking systems is proposed in [13,9]. Also, with respect to control systems we can find in other applications such as control of hard disk drive servo systems [15], control of an orbital Earth observing system [11], control of a two-axis sun following device [12,14], etc.

The problem of inertial stabilization is also an important issue in the field of aeronautical and navigational systems, among others. There are many applications in which a variable orientation relative to an inertial frame needs to be controlled. Some examples are automatic aircraft control, torpedo steering mechanisms [4], gaze stabilization for visual servoing [10], planetary gear transmission systems [6], humanoid robot control [17] and

amusement devices. In all of these cases, inertial stabilization requires measurement feedback from a gyroscopic sensor located on the mobile platform, which usually provides the velocity of a body with respect to the inertial frame.

This paper deals with the design and implementation of control structures for an industrial two-degree-of-freedom (2-DOF) platform, which rests on a base plate whose orientation can be arbitrarily modified. This allows us to emulate the disturbances in the intended final environment, such as the platform on board a ship, for instance. Cameras that need to be stabilized in the presence of different kind of perturbations are mounted on this type of platforms.

This control application was implemented in two different operation modes:

- A *non-inertial position control mode* in which the angular positions are the controlled variables. For this mode, a switching control strategy is proposed in order to reduce the undesirable consequences of the non-linear friction effects. One of the most noticeable effects on the controlled system due to friction is the presence of a limit cycle around the steady-state position values. The switching strategy consists of using a particular control law suitable for large displacements and switching to another control law when the platform angles are close to their reference values. This second controller is intended to reduce the steady-state error, that is, the amplitude of the mentioned limit cycle.
- An *inertial rate control mode*, where the inertial velocities of the platform are to be controlled. In this mode, we propose a master–slave control structure, combined with a gain-scheduling strategy. The inner control loop attempts to reject

^{*} Corresponding author. Tel.: +34 954487350; fax: +34 954487340.

E-mail addresses: rubio@esi.us.es (F.R. Rubio), mortega@esi.us.es (M.G. Ortega), gordillo@esi.us.es (F. Gordillo), vargas@cartuja.us.es (M. Vargas).

friction disturbances, while the outer control loop is designed for appropriate tracking performance of velocity references.

As a matter of fact, the proposed control techniques in this paper was part of some work developed under contract for a industrial company, that incorporate this controller in the control of a radar platform. Due to the character of this work, this application of the controller cannot be published, and only simulation and application in a small platform are permitted for publication.

The remainder of the paper is organized as follows: In Section 2, descriptions of the physical platform and the corresponding model used for controller design are given. The strategies followed for controller design in both operating modes are presented in Section 3. Section 4 gives some simulation results with the proposed control structures. Section 5 presents some details about the hardware implementation of the control system as well as some experimental results from the real platform. Finally, in Section 6, the paper ends with some conclusions about the study presented.

2. System description

The system considered in this paper is the industrial 2-DOF platform shown in Fig. 1a. It consists of two main structural units: the *base*, whose position is determined by the *azimuth angle* ψ , and the *main body*, whose coordinate is the *elevation angle* θ . These angles are both depicted in the platform scheme presented in Fig. 1b. Each revolution axis is equipped with a current controlled DC brushless motor with a brake and gear reduction. Additional mass can be added in the elevation axis in order to modify the system behavior.

Two optical fiber gyros are available for the inertial control. The gyros are located in the elevation axis, so the inertial velocity measure for the azimuthal axis is modified when the elevation axis moves. This dependency can be overcome by a projection of the measure in the orientation axis with

$$\dot{\psi}_i = \frac{\dot{\psi}_{ig}}{\cos(\theta)} \tag{1}$$

where $\dot{\psi}_{ig}$ is the gyro measurement, θ is the elevation angle and $\dot{\psi}_i$ is the modified measurement.

Besides this, two pistons arranged in a quadrature fashion, independently driven by two velocity-controlled electrical motors, were included in the system. This allows us to introduce some disturbances with respect to the orientation of the base plate holding the 2-DOF platform.

Fig. 2 shows a schematic diagram of the 2-DOF platform. The platform orientation and elevation rates ($\dot{\psi}$ and $\dot{\theta}$, respectively) can be driven by means of two input torques: τ_ψ for the orientation axis and τ_θ for the elevation axis. Nevertheless, the available input signals being considered in this work are actually voltage signals. Thus, henceforth τ_ψ and τ_θ have to be understood as such and measured in volts.

Some dynamic behavior is involved in the gyro measures. The angular velocities of the non-inertial base plate, $\dot{\psi}_c$, $\dot{\theta}_c$ and $\dot{\phi}_c$ (orientation, elevation and yaw, respectively), implicit in the gyro measures, are considered as disturbances to be rejected in the regulation of the inertial platform velocities ($\dot{\psi}_i$ and $\dot{\theta}_i$).

Prior to the controller synthesis stage, it is necessary to obtain a model of the platform. The dynamic equations of the system can be obtained from Lagrange's equations of motion. In particular, the Lagrangian of the system under consideration is given by

$$L = T - V = \frac{1}{2}(\dot{\psi}^2(I_{zz_1} + I_{xx_2} \sin^2(\theta)) + I_{zz_2} \dot{\theta}^2) + I_{yy_2} \dot{\theta}^2 \tag{2}$$

where T and V are the kinetic and potential energy, respectively. I_{zz_1} stands for the moment of inertia of the first joint along its own axis (Z direction), I_{xx_2} , I_{yy_2} , I_{zz_2} are the moments of inertia of the elevation axis, along directions X , Y and Z , respectively.

Taking into account that the load of the elevation axis is concentrated along the shaft, the potential energy can be considered invariant and hence may be discarded from the equations. From the Lagrangian formulation, the following dynamic model of the 2-DOF platform derived:

$$\begin{cases} \tau_\psi = \ddot{\psi}(I_{zz_1} + \sin^2(\theta)I_{xx_2} + \cos^2(\theta)I_{zz_2}) + \dot{\psi}\dot{\theta}\sin(2\theta)(I_{xx_2} - I_{zz_2}) + F_\psi(\dot{\psi}) \\ \tau_\theta = \ddot{\theta}I_{yy_2} - \frac{1}{2}\dot{\psi}^2\sin(2\theta)(I_{xx_2} - I_{zz_2}) + F_\theta(\dot{\theta}). \end{cases} \tag{3}$$

Functions $F_\psi(\dot{\psi})$ and $F_\theta(\dot{\theta})$ introduce friction torques in the orientation and elevation axes, respectively. A static, asymmetric

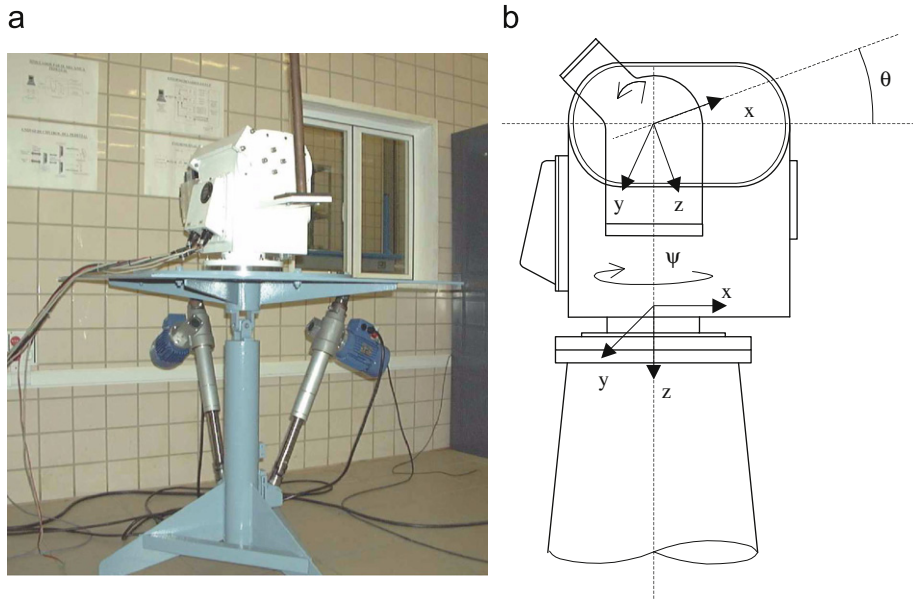


Fig. 1. Two degree-of-freedom platform. (a) Picture; (b) scheme.

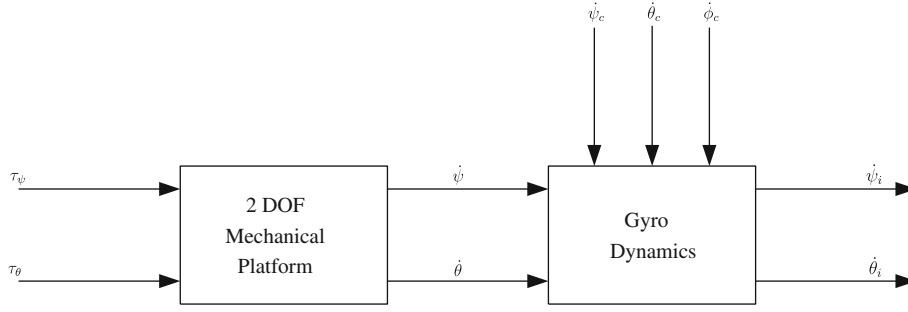


Fig. 2. Block diagram of the system model.

Table 1

Estimated values of the parameters of the platform model.

Parameter	Azimuth	Elevation	Units
I_{zz}	0.02	–	V/(rd/s ²)
$I_{xx}-I_{zz}$	–	≈ 0	V/(rd/s ²)
I_{yy}	–	0.018	V/(rd/s ²)
F_v^+	0.11	0.26	V/(rad/s)
F_v^-	0.12	0.20	V/(rad/s)
F_s^+	0.28	0.7	V
F_s^-	0.19	0.5	V
F_c^+	0.48	0.57	V
F_c^-	0.42	0.88	V

friction model, giving a nonlinear relationship between friction torque and shaft velocity has been identified [5]. The expression that computes the friction torque for each degree of freedom, $q = \psi, \theta$, is

$$F_q(\dot{q}) = [F_v^+ |\dot{q}| + F_c^+ + (F_s^+ - F_c^+) e^{-|\dot{q}|B^+}] \text{sgn}^+(\dot{q}) + [F_v^- |\dot{q}| + F_c^- + (F_s^- - F_c^-) e^{-|\dot{q}|B^-}] \text{sgn}^-(\dot{q}) \quad (4)$$

where F_c is the Coulomb friction (as the friction model is asymmetric, different values are expected for positive and negative directions), F_v the viscous friction, F_s the static friction and B is the exponent of the Stribeck effect. The sign functions are defined as follows:

$$\text{sgn}^+(\dot{q}) = \begin{cases} 1 & (\dot{q} \geq 0) \\ 0 & (\dot{q} < 0) \end{cases} \quad \text{sgn}^-(\dot{q}) = \begin{cases} 0 & (\dot{q} \geq 0) \\ -1 & (\dot{q} < 0) \end{cases}$$

The parameters of the platform model were estimated from some experiments on the real system, through an RLS algorithm [5]. The values found for these parameters are given in Table 1.

In order to implement an inertial control of the platform, the gyro kinematics and dynamics need to be modeled. With regard to kinematics, it is known that the gyro measures a combination of the platform velocity and the base plate velocity, according to the following expressions:

$$\dot{\psi}_i^m = (\dot{\psi} + \Omega_{c_x}) \cos(\theta) + \Omega_{c_y} \sin(\psi) \sin(\theta) + \Omega_{c_z} \cos(\psi) \sin(\theta)$$

$$\dot{\theta}_i^m = \dot{\theta} + \Omega_{c_y} \cos(\psi) + \Omega_{c_x} \sin(\psi)$$

where $\Omega_c = [\Omega_{c_x}, \Omega_{c_y}, \Omega_{c_z}]^T$ is the angular velocity vector of the base plate, measured from an inertial reference frame. The components of this vector can be computed from the orientation, elevation and yaw angles (ψ_c , θ_c and ϕ_c) as follows:

$$\Omega_{c_x} = \dot{\phi}_c - \dot{\psi}_c \sin(\theta_c)$$

$$\Omega_{c_y} = \dot{\theta}_c \cos(\phi_c) + \dot{\psi}_c \cos(\theta_c) \sin(\phi_c)$$

$$\Omega_{c_z} = -\dot{\theta}_c \sin(\phi_c) + \dot{\psi}_c \cos(\theta_c) \cos(\phi_c)$$

The dynamic gyro model has been described by a second-order transfer function, following the recommendations given in [8]

$$G_g(s) = \frac{\omega_g^2}{s^2 + 2\delta_g \omega_g s + \omega_g^2} \quad (5)$$

Consequently, the true gyro measurements are obtained from the application of this transfer function to the values given by the kinematic model, i.e.

$$\dot{\psi}_i = G_g(s) \dot{\psi}_i^m, \quad \dot{\theta}_i = G_g(s) \dot{\theta}_i^m$$

3. Controller design

Two different control approaches were tried out on the 2-DOF platform. The first one focuses on position control of the platform in the absence of inertial disturbances. In this case, the aim is to cancel the non-linear effects mainly due to friction forces, which are more apparent during positioning experiments (at low or null velocities). As mentioned before, one of the most noticeable of these effects is the existence of a limit cycle, coming from the dead zone produced by stick-slip effect.

The second control strategy is intended for inertial rate control, where inertial velocities, $\dot{\psi}_i$ and $\dot{\theta}_i$, are controlled to converge to their references, $\dot{\psi}_i^r$ and $\dot{\theta}_i^r$, in the presence of inertial disturbances coming from orientation changes in the base plate. In addition, disturbances due to friction effects must be appropriately rejected. As an additional specification in this case, the maximum error of the inertial position with a zero velocity setpoint must be bounded.

Each of these control strategies is described in below.

3.1. Position control mode

The pair of equations given in (3) shows the system coupling due to Coriolis and inertia terms. However, as a consequence of the high gear reduction present in the system, this coupling effect is greatly reduced. In particular, note the value of coefficient ($I_{xx}-I_{zz}$) in Table 1, which allows the non-linear terms in (3) to be neglected, resulting in

$$\tau_\psi = \ddot{\psi} I_{zz1} + F_\psi(\dot{\psi})$$

$$\tau_\theta = \ddot{\theta} I_{yy2} + F_\theta(\dot{\theta})$$

Therefore, independent joint control would be appropriate for our purposes. Furthermore, in order to get a simple linear model for each platform axis, only viscous friction is being maintained in the formulation, while the other terms are considered sources of disturbances to be rejected.

Hence, the controller will be designed according to the following linearized plant model:

$$G_{p,q}(s) = \frac{K_q}{s(s+a_q)}, \quad q = \psi, \theta \quad (6)$$

with static gain $K_q = K_{\tau_q}/I_q$ and a stable pole corresponding to $a_q = F_{v_{min}}/I_q$. K_{τ_q} is the torque constant of the corresponding axis servomotor, and I_q is equal to I_{zz_1} or I_{yy_2} for the orientation or elevation axis, respectively. Finally, $F_{v_{min}}$ is taken as $F_{v_{min}} = \min\{F_v^+, F_v^-\}$ for the corresponding axis.

The design specifications require that the system reaches, a position inside a region close to the reference as quickly as possible. Moreover, the amplitude of the limit cycle due to stick-slip phenomenon must be bounded as another specification. These requirements are achieved by means of a switching strategy with two different linear control laws. The first one is called *large-displacement controller* (henceforth called $C_{ld}(s)$), which brings the states near their setpoints. The second law is the *short-displacement controller* (henceforth called $C_{sd}(s)$), which is in charge of state regulation around the references.

The *large-displacement controller* can be obtained by imposing a particular closed-loop dynamic behavior. If a *proportional-derivative* structure is employed, the controller $C_{ld}(s)$ follows the expression:

$$u_{ld}(t) = K_p e(t) - K_D \dot{q}(t) \quad (7)$$

where $e(t) = q^r(t) - q(t)$ (with $q = \{\psi, \theta\}$), is the tracking error and $\dot{q}(t)$ is the velocity of the corresponding axis. Thus, a closed loop transfer function can be obtained in the form:

$$G_{bc} = \frac{KK_p}{s^2 + (a + KK_D)s + KK_p} \quad (8)$$

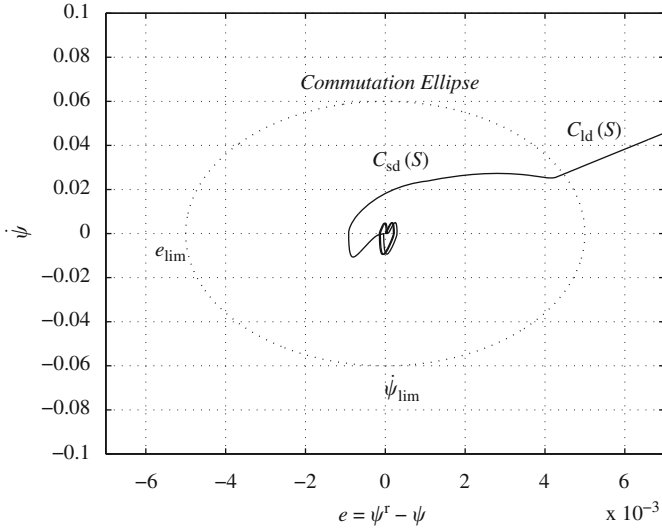


Fig. 3. Commutation boundary for the switching strategy ($q = \psi$).

As has already been mentioned, the goal of this controller is to bring the system to a state near the reference. It is clear that the controller parameter K_p should be chosen large enough to overcome the dead zone that results from static friction, so the steady-state error remains inside an acceptable band. In particular, this steady-state error, e_{ss} , can be reduced through the proportional gain according to

$$e_{ss} \approx \frac{F_c}{K_p} \quad (9)$$

where F_c is the Coulomb friction. This condition may be even more restrictive than the one imposed by the rise time of the closed-loop response.

The controller parameter K_D , can be computed by forcing a critically damped, second-order, closed-loop response. This condition gives the following expression for K_D :

$$K_D = \frac{2\sqrt{KK_p} - a}{K} \quad (10)$$

Since the goal of the preceding controller is to bring the platform angles near to their references, and then switch the control law to the *short-displacement controller*, an elliptic commutation boundary was defined to perform the controller switching action. This boundary is given by the equation:

$$\frac{e^2}{e_{lim}^2} + \frac{\dot{q}^2}{\dot{q}_{lim}^2} = 1 \quad (11)$$

where e_{lim} and \dot{q}_{lim} are the radii of the ellipse. This concept is illustrated in Fig. 3.

As shown in the figure, when the system reaches the commutation ellipse, the control law is switched to the $C_{sd}(s)$, which is designed as a *proportional-integral-derivative* structure:

$$u_{sd}(t) = K_p e(t) - K_D \dot{q}(t) + K_I \int_0^t e(\tau) d\tau \quad (12)$$

The PID gains of this controller are adjusted in order to control the amplitude of the limit cycle that results from the stick-slip phenomenon. The amplitude, A_{lc} , and the period, T_{lc} , of this limit cycle can be estimated theoretically through the following expressions [5]:

$$A_{lc} \approx \frac{F_s - F_c}{2K_p}, \quad T_{lc} \approx \frac{4K_p F_s + F_c}{K_I F_s - F_c} \quad (13)$$

Consequently, after the specification of this amplitude and period, a combination of controller gains may be obtained constrained to the previous relationships.

3.2. Velocity control mode

As has been noted, the purpose in this control mode is to cause the inertial platform velocities to converge to their references, in the presence of inertial disturbances coming from orientation changes in the base plate, and disturbances of a different nature, those due to friction effects.

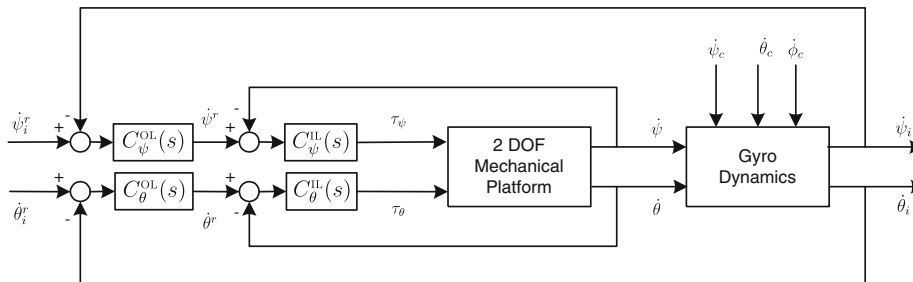


Fig. 4. Master-slave control structure.

Given the required specifications and the dynamics of the gyro sensor, the controller cannot be successfully implemented in a single loop form. This is due to the high controller gain required to reject friction disturbances, which produces an unstable closed loop when the gyro dynamics are introduced.

In order to solve this problem, we propose a master–slave control structure (see Fig. 4). An inner velocity loop is built with the estimation of the velocity, while an outer loop is closed with the gyro measurements. Following this structure, the *inner controllers*, $C_{\psi}^{IL}(s)$ and $C_{\theta}^{IL}(s)$, are designed in such a way that the nonlinear effects present in the system are rejected by the inner

loop, while the *outer controllers*, $C_{\psi}^{OL}(s)$ and $C_{\theta}^{OL}(s)$, are synthesized in order to reject the disturbances produced by the base-plate motion.

Also a structure with a friction compensator [1] was tested in simulation and similar results were obtained. Taking into account the practical aspects of the controller implementation, we opted for the master–slave structure of the Fig. 4.

For this control structure to perform appropriately, the inner loop should have a faster dynamic behavior than the external loop. By the way, this same principle will allow the controllers to be independently designed.

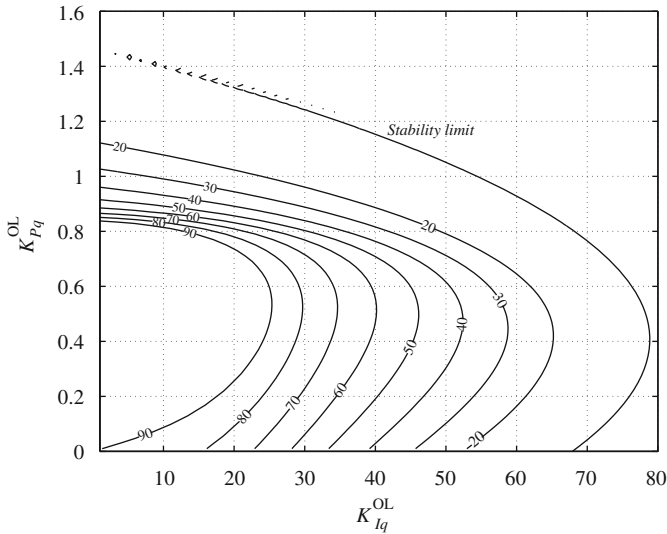


Fig. 5. Phase margin of the system as a function of the outer-controller gains, K_{Pq}^{OL} and K_{Iq}^{OL} .

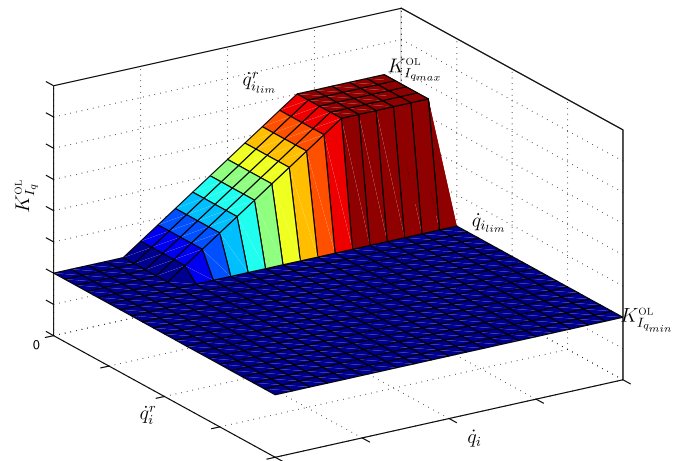


Fig. 6. Correction for the K_{Iq}^{OL} parameter of the external control loop

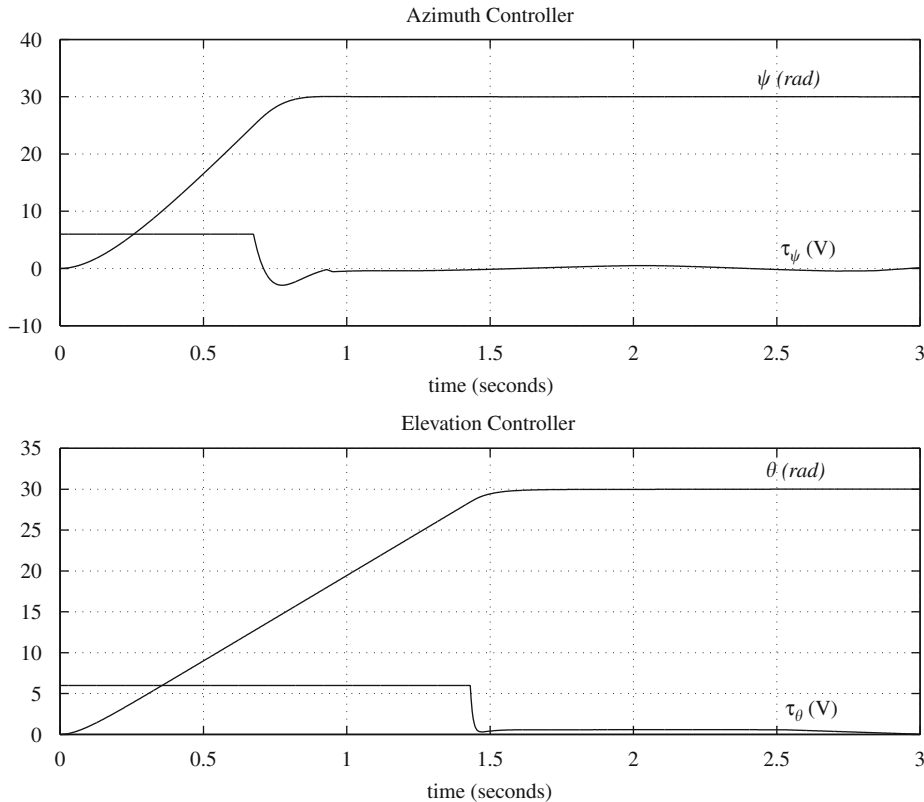


Fig. 7. Time response in position control mode.

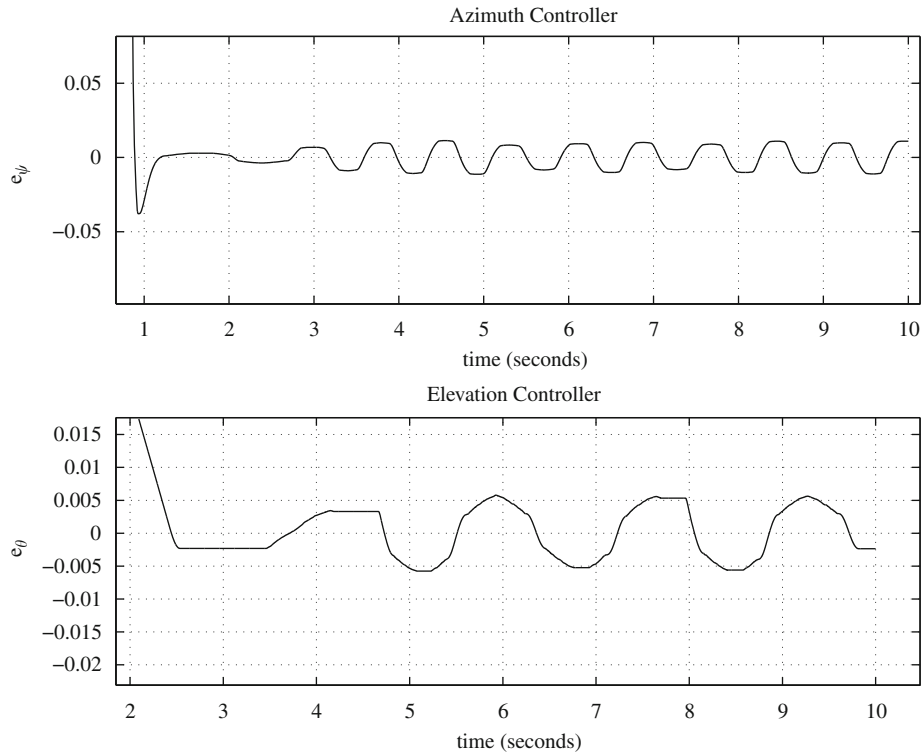


Fig. 8. Limit cycles around the reference in position control mode.

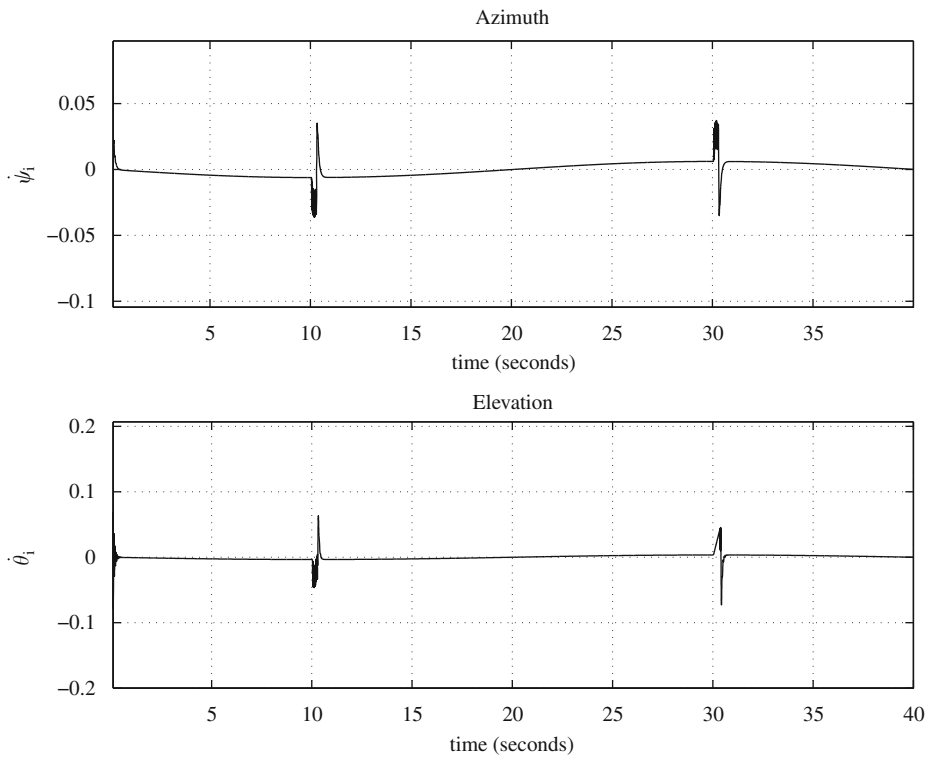


Fig. 9. Inertial velocity response for $\dot{\psi}^r = \dot{\theta}^r = 0$, including external disturbances.

A *proportional-integral* structure is chosen for inner controllers $C_q^{IL}(s)$ ($q = \psi, \theta$). Their gains are computed from

$$K_{P_q}^{IL} = \frac{2\delta\omega}{a_q} \frac{1}{K_q}, \quad K_{I_q}^{IL} = \frac{\omega^2}{K_q a_q} \quad (14)$$

where ω and δ are now the natural frequency and the damping factor, respectively, corresponding to the desired response of the inner loop. Parameters K_q and a_q are the gain and the pole of the linear part of the system given in (6).

Due to the nonlinear influence of the actuator saturation, the system has an undesirable overshoot when large reference

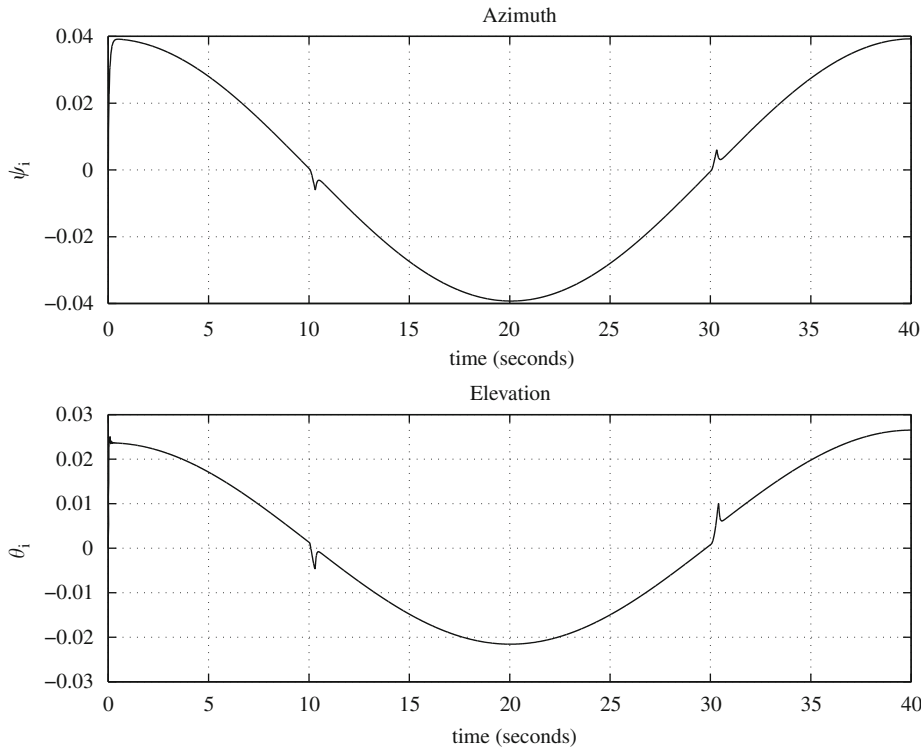


Fig. 10. Inertial position response for external disturbances and $\dot{\psi}^r = \dot{\theta}^r = 0$.

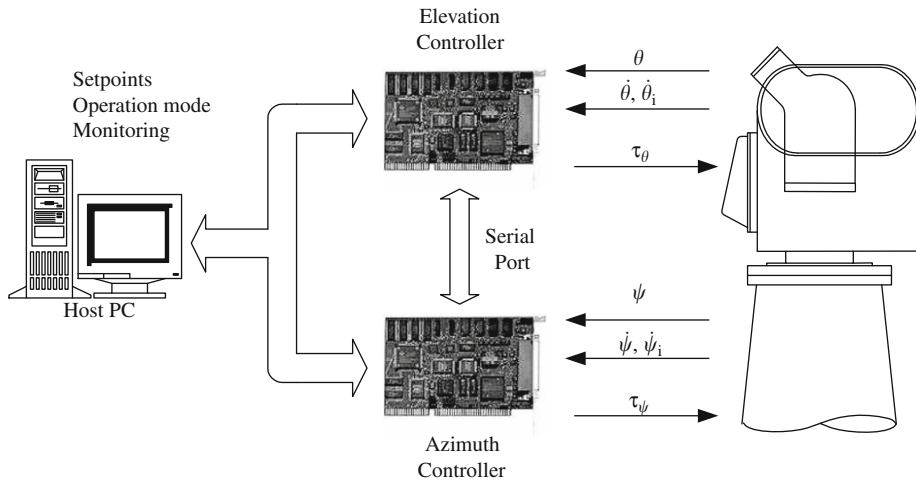


Fig. 11. Hardware implementation of the controllers.

changes are given. Hence an anti-windup strategy [3] was added to the control scheme in order to allow the control signal to leave its saturation state as soon as possible.

With regard to the inertial velocity outer loop, a gain-scheduling control was implemented [2]. In particular, a *proportional-integral* control structure has also been chosen for the outer controllers ($C_q^{OL}(s)$, $q = \{\psi, \theta\}$), whose gains may vary depending on the operating point. This way, it is possible to fulfill the desired specifications in different working regions.

In order to give a practical criterion for tuning the outer-controller gains, the theoretical stability of the controlled system was analytically studied. The phase margin provided by the external controllers associated with their proportional and integral parameters (to be referred as K_p^{OL}, K_i^{OL}) is shown in Fig. 5. The limit of the closed-loop stability can be symbolically

computed as a function of the outer controller gains. This limit is defined by the following equation:

$$0 = \frac{\gamma_{00} + \gamma_{11}K_{p0}K_{i0} + \gamma_{21}K_{p0}^2K_{i0} + \gamma_{30}K_{p0}^3 + \gamma_{20}K_{p0}^2 + \gamma_{10}K_{p0} + \gamma_{01}K_{i0} + \gamma_{02}K_{i0}^2}{\delta_{00} + \delta_{20}K_{p0}^2 + \delta_{10}K_{p0} + \delta_{01}K_{i0}} \quad (15)$$

where δ_{ij} and γ_{ij} are

$$\begin{aligned} \gamma_{00} &= \alpha_1^2\alpha_0 - \alpha_3\alpha_2\alpha_1\alpha_0 + \alpha_3^2\alpha_0^2 \\ \gamma_{11} &= -\alpha_3\alpha_2\beta_1^2 - \alpha_2\beta_1\alpha_0 + 2\beta_1^2\alpha_1 - 2\alpha_3\alpha_0^2 + 2\alpha_3^2\alpha_0\beta_1 \\ \gamma_{21} &= \beta_1^3 \\ \gamma_{30} &= \beta_1^2\alpha_0 \\ \gamma_{20} &= -\alpha_3\alpha_2\beta_1\alpha_0 + 2\beta_1\alpha_1\alpha_0 + \beta_1^2\alpha_0 + \alpha_3^2\alpha_0^2 \\ \gamma_{10} &= \alpha_1^2\alpha_0 - \alpha_3\alpha_2\beta_1\alpha_0 + 2\alpha_3^2\alpha_0\alpha_0 - \alpha_3\alpha_2\alpha_1\alpha_0 + 2\beta_1\alpha_1\alpha_0 \\ \gamma_{01} &= -\alpha_2\alpha_1\alpha_0 - \alpha_3\alpha_2\alpha_1\beta_1 + \alpha_0\alpha_3\alpha_2^2 - 2\alpha_3\alpha_0^2 + 2\alpha_3^2\beta_1\alpha_0 + \alpha_1^2\beta_1 \end{aligned}$$

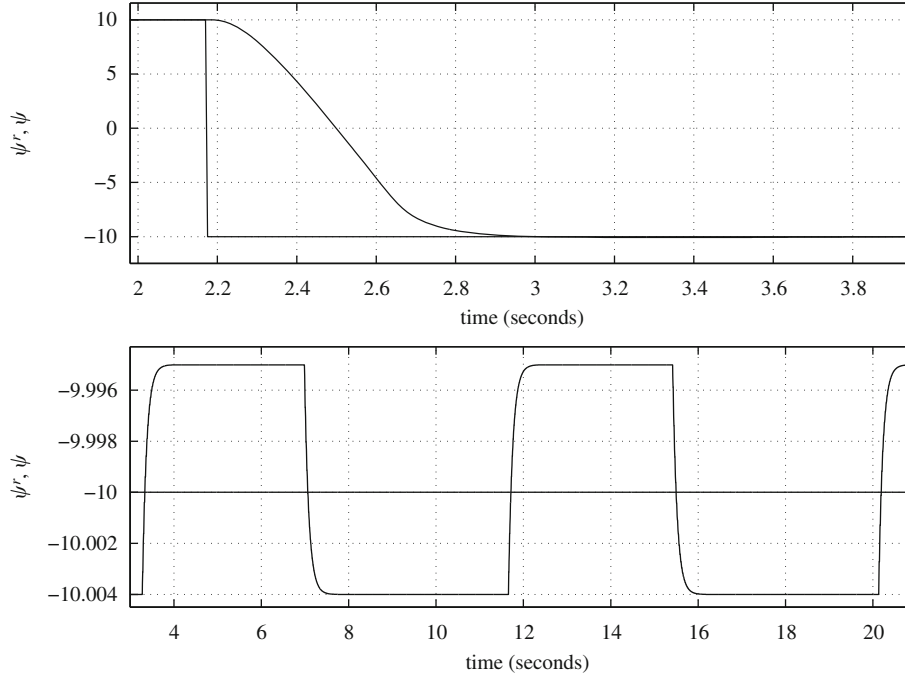


Fig. 12. Position control mode: step response for azimuthal axis.

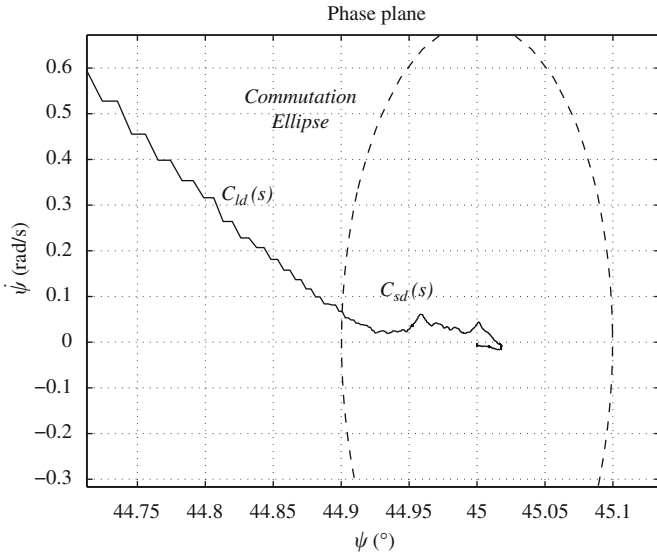


Fig. 13. Position control mode: switching of the position controllers.

$$\begin{aligned}
 \gamma_{02} &= \alpha_0^2 - 2\alpha_3\beta_1\alpha_0 + \alpha_3^2\beta_1^2 \\
 \delta_{00} &= -\alpha_1^2 + \alpha_3\alpha_2\alpha_1 - \alpha_3^2\alpha_0 \\
 \delta_{20} &= \beta_1^2 \\
 \delta_{10} &= -\alpha_3^2\alpha_0 + \beta_1\alpha_3\alpha_2 - 2\beta_1\alpha_1 \\
 \delta_{01} &= -\alpha_3^2\beta_1 + \alpha_3\alpha_0
 \end{aligned} \tag{16}$$

The values of α_i and β_i can be calculated as a function of the internal-loop parameters as follows:

$$\begin{aligned}
 \alpha_0 &= K_q K_{I_q}^{ll} \omega_g^2 \\
 \alpha_1 &= K_q K_{P_q}^{ll} \omega_g^2 + a_q \omega_g^2 + 2K_q K_{I_q}^{ll} \delta_g \omega_g \\
 \alpha_2 &= 2K_q K_{P_q}^{ll} \delta_g \omega_g + K_q K_{I_q}^{ll} + \omega_g^2 + 2a_q \delta_g \omega_g
 \end{aligned}$$

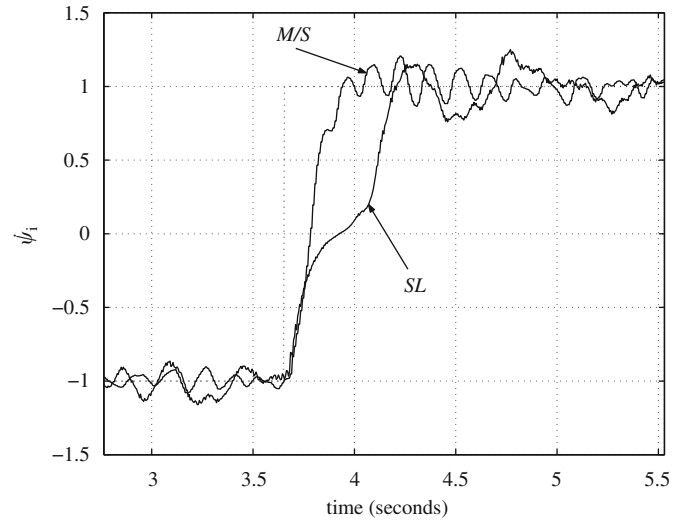


Fig. 14. Inertial velocity step responses.

$$\begin{aligned}
 \alpha_3 &= K_q K_{P_q}^{ll} + 2\delta_g \omega_g + a_q \\
 \beta_1 &= K_q K_{P_q}^{ll} \omega_g^2
 \end{aligned} \tag{17}$$

This stability limit was computed using the models given by (5) and (6), and the internal controller gains obtained from (14).

The operation region of the controller was divided according to the magnitudes of setpoints and shaft velocities. The gain-scheduling strategy is introduced at this point. Basically, the system needs to operate in two regions: a *high rate mode* and a *low or zero rate mode*, according to the reference magnitude. In the second mode, the platform should move slowly in order to compensate for the base plate motion. In this mode, the integral gain is modified according to the axis velocity. This results in an improvement in the system stabilization. The operation regions of the outer loop are shown in Fig. 6 (again, $q = \{\psi, \theta\}$).

4. Simulation results

In the following experiments, the preceding controllers were tested on the nonlinear system model (3), together with the dynamic model of the gyro. A static and asymmetric friction model, whose values were given in Table 1, is used for position-mode and velocity-mode simulations.

Regarding the *position control mode*, Fig. 7 shows the step responses in the orientation and elevation axes, as well as the control signals supplied by the controllers. It can be seen that when large setpoint changes are required, the *large-displacement controllers* produce a saturated control signal, accelerating and decelerating the system quickly.

The effects produced by the *short-displacement controllers*, which cannot be perceived in Fig. 7, are presented in Fig. 8. When the system is close to the reference, these controllers improve the steady-state error and take the system to a limit cycle, the amplitude of which is in accordance with the required precision.

With respect to the *velocity control mode*, Figs. 9 and 10 show how the inertial velocity controller performs when a null reference is given. In order to include the motion of the non-inertial base plate, the following disturbance signals were added in this simulation:

$$\begin{aligned}\psi_c = \phi_c = \theta_c &= 0.0830 \sin\left(0.08t - \frac{\pi}{2}\right) \\ \dot{\psi}_c = \dot{\phi}_c = \dot{\theta}_c &= 0.00664 \cos\left(0.08t - \frac{\pi}{2}\right)\end{aligned}\quad (18)$$

Small disturbances were chosen, causing the platform to move at low velocities, where friction is more relevant. Fig. 9 shows that the inertial velocities, $\dot{\psi}_i$ and $\dot{\theta}_i$, actually remain close to zero, and just a few velocity peaks can be observed when the corresponding motor velocity (i.e., non-inertial measures $\dot{\psi}$ and $\dot{\theta}$) reaches zero. At these instants, although the motor shaft is stopped due to the friction torque, the disturbances can be rejected.

Fig. 10 shows the inertial position of the platform when the reference is a zero velocity. It can be seen that the positions oscillate due to the non-perfect cancelation of the disturbances.

5. Experiments on the real platform

The control structures described throughout the paper were also implemented in the hardware equipment devoted to the control of the physical platform. Fig. 11 shows the hardware used in order to implement the controllers. Two controller boards were used for the implementation of these controllers. The boards have a real-time kernel running in a TMS320C31 DSP from Texas Instruments and several I/O interfaces. The elevation and orientation control algorithms run separately on each board, so a connection between the processors was established and the dynamic variables can be interchanged. This connection is implemented as a high-speed serial port. A host computer is used for monitoring and data acquisition purposes.

The system behavior in *position control mode* is presented in Figs. 12 and 13. The azimuthal response, while tracking large step-like changes in the reference is presented in Fig. 12. The saturation effects can be appreciated in the upper plot of this figure. The lower plot enables us to appreciate the amplitude and period of the limit cycle around the steady-state values. The switching controller allows for the achievement of very good performance in reference tracking, despite the unmodeled platform dynamics. Fig. 13 shows the switching from the *large-displacement controller* to the *short-displacement controller* for the azimuthal axis in the real system.

The *velocity control mode*, described in Section 3.2, was tested in the real platform as well. Fig. 14 shows the velocity step response in the azimuthal axis with two different control strategies. The response labeled as *M/S* corresponds to the *master-slave* structure proposed in this paper, while the one marked as *SL* (i.e. *single loop*) corresponds to a single controller with no inner loop. The proposed controller demonstrates better performance as long as the internal loop allows the rejection of the system disturbances. These disturbances are mainly created by the stick-slip phenomenon when there are velocity reversals.

6. Conclusions

This paper presents the design and implementation of two different control structures, corresponding to position and inertial velocity regulation of a two-degree-of-freedom gyroscopic platform, mounted on a base plate whose orientation can be modified at will. Also, the controller structure proposed in this paper has actually been used in a real radar gyroscopic platform.

A switching control law proved to be appropriate for position control mode, as it distinguished between large and short displacements. A commutation ellipse in the phase plane was defined as the switching boundary.

In the case of the velocity control mode, a master-slave structure was proposed. In this structure, the aim of the inner controller is the rejection of disturbances due to non-linearities of the system, while the outer controller (a gain scheduling control law) is in charge of the rejection of disturbances due to movements of the base plate.

Simulation results, using a nonlinear model of the system, including gyro dynamics and a static, asymmetric, non-linear friction model, as well as experimental results, have been presented. These experiments show that the system perform well; the controllers are capable of dealing with changes in the system dynamics caused by the different operating points.

The contents of the paper reveal how the control of position and inertial velocities of the 2-DOF platform can be solved by simple control structures, despite the existence of important nonlinear effects in the system.

Acknowledgments

The authors would like to acknowledge MCyT-FEDER for funding this work under Grants DPI2009-09961 and DPI2007-64697. The authors would also like to acknowledge to Carlos Pérez for his collaboration during the project “Control of Gyro-stabilized Platforms”.

References

- [1] Armstrong-Hélouvy B, Dupont P, Canudas-de-Wit C. A survey of models, analysis tools and compensation methods for the control of machines with friction. *Automatica* 1994;30(7):1083–138.
- [2] Åström KJ, Wittenmark B. *Adaptive control*. Reading, MA: Addison-Wesley; 1989.
- [3] Åström KJ, Wittenmark B. *Computer-controlled systems. Theory and design*, 3rd ed. Englewood Cliffs, NJ: Prentice-Hall; 1997.
- [4] Becherini G. Gyroscopic stabilization of launch package in induction type coilgun. *IEEE Transactions on Magnetics* 2001;37(1):116–22.
- [5] Canudas-de-Wit C, Åström KJ, Sorin M. Slides of the workshop control of systems with friction. Presented at: the IEEE conference on decision and control CDC'98, December Florida, USA, and at the IEEE conference on control applications CCA'99, August 22–27, Hawaii, USA, 1999 <http://www.lag.ensieg.inpg.fr/canudas>.
- [6] Dewdney P, Nahon M, Veidt B. The large adaptive reflector: a giant radio telescope with an aero twist. *Canadian Aeronautics and Space Journal* 2002;48(4):239–50.

- [7] Guesalaga A. Modelling end-of-roll dynamics in positioning servos. *Control Engineering Practice* 2004;12(1):217–24.
- [8] Li B, Hullender D. Self-tuning controller for nonlinear inertial stabilization systems. *IEEE Transactions on Control Systems Technology* 1998;6(3): 428–34.
- [9] McInroy JE, Neat GE, O'Brien JF. A robotic approach to fault-tolerant precision pointing. *IEEE Robotics & Automation Magazine* 1999;6(4): 24–37.
- [10] Panerai F, Sandini G. Oculo-motor stabilization reflexes: integration of inertial and visual information. *Neural Networks* 1998;11:1191–204.
- [11] Robeck LS, Rathbun DB, Lehman DH. Precision pointing control for an orbital earth observing system. *IEEE Control Systems* 1991;11(3):46–52.
- [12] Roth P, Georgiev A, Boudinov H. Cheap two axis sun following device. *Energy Conversion & Management* 2004;46(7–8):1179–92.
- [13] Rubio FR, Aracil J. Design of a combined tracking control system. *Control Engineering Practice* 1997;5(1):23–31.
- [14] Rubio FR, Ortega MG, Gordillo F, López-Martínez M. Application of new control strategy for sun tracking. *Energy Conversion and Management* 2007;48(7):2174–84.
- [15] Venkataramanan V, Chena BM, Leea TH, Guob G. A new approach to the design of mode switching control in hard disk drive servo systems. *Control Engineering Practice* 2002;10:925–39.
- [16] Vivas C, Canudas-de-Wit C, Rubio FR. Gain-scheduled control of systems with dynamic friction. In: 41th IEEE conference on decision and control, Las Vegas, Nevada, 2002. p. 89–94.
- [17] Wong TCF, Hung YS. Stabilization of biped dynamic walking using gyroscopic couple. *IEEE international joint symposia on intelligence and systems*, 1996. p. 102–8.